Austin Tuan - September 26, 2016

Studying the Dependence of Dark Matter Halo Density Distribution on Environment

ABSTRACT

Despite it making up nearly 30% of matter in our universe, very little is known even today about dark matter and its role in the creation and evolution of stars and galaxies. In the past two decades, though, advancements in computing have made it possible for researchers to simulate the evolution of the universe and dark matter halos from the Big Bang to the present. Central to the study of dark matter halos, and one of the key applications of these cosmological simulations, is understanding how halos interact with each other. In order to gain insight into the effects of environment on halo evolution, we created a new equation that could characterize halos whose density distributions deviate from the standard Navarro-Frenk-White (NFW) profile. Using data from the Bolshoi-Planck cosmological simulation, we optimized our fit for each dark matter halo, and ensured the fidelity of our analysis by also comparing NFW optimization values. We then correlated these values with other properties of halos that are dependent on environment. By storing our values in the halo catalog, we make it possible for researchers in the future to access our analysis and expand the study to new halo properties. Through our work, we present two causes of divergence from the normal density distributions of dark matter halos, and lay the groundwork for future investigation into the circumstances that produce irregular halos.

1 INTRODUCTION

According to current estimates, ordinary matter makes up only 4% of the density of our universe. Dark matter, on the other hand, makes up 26%. Therefore the study of its origins and properties is a rapidly expanding field in astronomy, and one that is crucial to understanding the evolution and structure of the universe. Because dark matter does not absorb or emit light, we must rely on simulations to study it (Behroozi et al. 2013). In the last few decades, research into dark matter has been greatly advanced by the development of modern-day supercomputers, which have enabled cosmological simulations (Klypin et al. 2014, Prada et al. 2012). Such simulations make predictions, and thus far all the predictions that have been tested have been confirmed. As computing power continues to grow, scientists will get a clearer picture of the role that dark matter plays in the universe.

Although undetectable to the eye, the existence of cold dark matter (CDM) was theorized in the 1980s. CDM is a component of the now-standard Lambda-Cold Dark Matter (ΛCDM) cosmological model. CDM explains the significant disparities discovered between the large gravitational effects of large astronomical structures and the smaller masses of their luminous components (Blumenthal et al. 1984). Because of quantum fluctuations in density that were exponentially inflated in the moments after the Big Bang, masses of dark matter clump together gravitationally to make dark matter halos, which contain baryonic galaxies at their center. These halos themselves also clump together, creating web structures of varying density—voids, walls, filaments, and nodes—rather than a uniformly dense universe (Schramm 1993). At the earliest stages of the universe, halos accreted mass rapidly. Dark matter halos are elongated along one axis, and can be approximated as prolate ellipsoids (Allgood et al. 2006). Halos continue to grow through mass accretion and mergers with other halos, but the rate of growth will slow as they age.

As a halo's mass increases, it becomes more spherical (Correa et al. 2015). In our research, we approximate all halos as spherical.

Since its development in 1996, the Navarro-Frenk-White (NFW) profile (Navarro, Frenk, & White 1996 & 1997) has served as the standard model of a halo's density distribution. Here ρ is density, r is radius, and both ρ_s and r_s are halo parameters:

$$\rho(r) = \frac{4\rho_s}{\frac{r}{r_s}\left(1+\frac{r}{r_s}\right)^2} \quad (1)$$

According to NFW, the slope of a density distribution when plotted in log space changes from -1 to -3 at the scale radius (r_s).

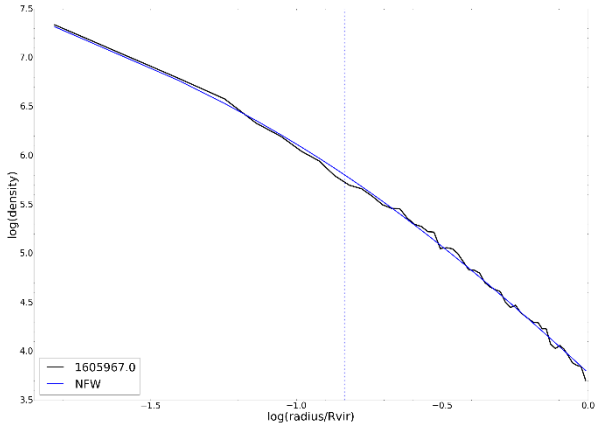

FIGURE 1. Density Distribution of a Dark Matter Halo. A plot of halo 1605967's density as a function of radius in log space. The standard NFW profile has been superimposed, showing the characteristic slope change from -1 to -3 at r_s, as denoted by the dotted blue line.

Run in 2013, the Bolshoi-Planck Simulation (Rodriguez-Puebla et al. 2016) became the most accurate cosmological simulation ever. Using parameters from the Planck satellite, the simulation modeled the movement of dark matter particles from the moments immediately after the Big Bang to the present day in a nonspecific region of the universe. In order to use the simulation's results, halos were identified using the Rockstar algorithm, which compiled the various properties of each halo at 180 timesteps into a table (Behroozi et al. 2012). When matched

to galaxies, the distribution of dark matter halos showed significant agreement with observations from the Sloan Digital Sky Survey. After multiple tests confirmed the accuracy of the simulation, researchers began to use its data in their study of the nature of dark matter halos.

Using these cosmological simulations, researchers discovered the phenomenon of tidal stripping between halos. Although most halos are at their peak mass in the present, some lower-mass halos have actually lost dark matter particles. These halos are product of tidal stripping, which are the consequences of gravitational forces that large, nearby halos exert on these low mass halos (Taylor & Babul 2001 & 2004). For two halos distance *D* apart, one larger and one smaller, the farthest that a particle accreting into the secondary halo can be so that it stays gravitationally bound to that halo is the Hill Radius, defined as:

$$R_{Hill} = D\left(\frac{M_{secondary}}{3M_{primary}}\right)^{1/3} \quad (2)$$

The smaller the distance, the stronger are the tidal forces, and thus the smaller is the Hill Radius (Hahn 2009). In this way, if a primary halo exerts a tidal force with $R_{Hill} \sim R_{secondary}$, mass accretion by the secondary halo is inhibited (Hearin, Behroozi, & van den Bosch 2016). Once tidal forces are strong enough, particles can even be unbound from the secondary halo, resulting in mass loss by that halo (Kampakoglou & Benson 2007). In the most extreme cases, entire halos can be swallowed up by the primary halo (Benson 2010). These phenomena—merging and stripping—are the driving forces of halo growth.

2 SIGNIFICANCE OF RESEARCH

Researchers have discovered that for a subset of halos in cosmological simulations, the NFW profile fits poorly to the distribution, either because the outside slope was too shallow or too steep compared to the NFW $1/r^3$ outer slope. In order to understand how these kinds of halos

emerge in the Bolshoi-Planck simulation, we characterize the outer slope as a halo property by fitting a new equation to replace the NFW function. Once these values were logged, we could correlate outer slopes with other properties, using the ID unique to each halo to access a comprehensive catalog of properties that have already been calculated by Rockstar. By also re-fitting NFW to our halos, we could also compare the quality of the two fits in relation to those properties. Moving forward, by appending these values to the halo catalog, we will have the ability to access the outer slope value as easily as we can the mass or radius of a halo, and facilitate the refinement of new profiles that seek to better describe the density distributions of dark matter halos.

3 PROCEDURE

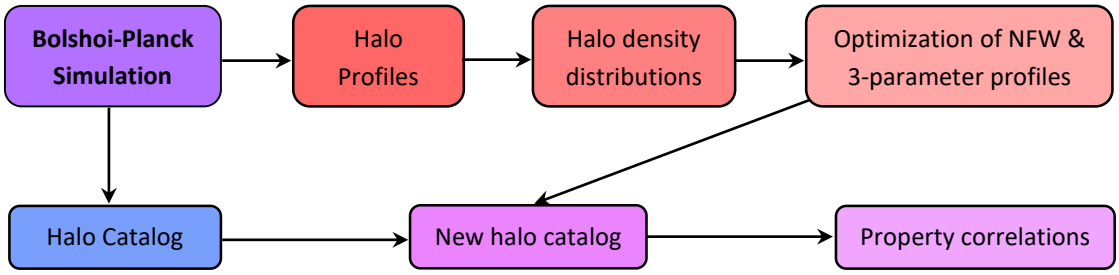

FIGURE 2. Procedural Flow Diagram. This is the procedure we took to create our plots.

Figure 2 visualizes the steps required to generate our results. All halos are taken from the Bolshoi-Planck simulation, and all halo data is taken from the tables produced by Rockstar from the simulation.

3.1 Density Profiles

Newly released halo profiles for the simulation expedited the creation of halo density distributions. To plot such a graph, radial bins are selected, and the density of dark matter particles inside each concentric ring is calculated for each bin. The technique used by the halo profiles chose

radii that would create similar numbers of bins encompassing equal numbers of particles. With these values compiled in a table, we no longer had to use particle data to construct plots for each halo, allowing us to expand the analysis to a larger number of halos than previously possible. Although halos are ellipsoidal, we calculated the volumes of each radial bin as spheres for simplicity. In line with previous research, the densities and radii were plotted on a log scale out to the virial radius, or outer boundary, of the halo. We then calculated our own NFW r_s and scale density, fitting each halo distribution to the profile using a least-squares optimization algorithm.

3.1.1 3-Parameter Fit

In order to characterize the outer slope, we modified the NFW profile to create another parameter. Taking a look again at the NFW equation (Equation 1), it establishes the linear slope change when graphed in log space by only rendering the second term of the denominator significant at $r > r_s$. At radii r much smaller than the scale radius r_s, only the exponent of the first term is active, so the slope is -1. Once $r > r_s$, the second term begins to have a larger effect, decreasing the slope to -3. By replacing the second exponent with a variable, we get Equation 4, which, from this point forward, we will call the 3-parameter fit:

$$\rho(r) = \frac{4\rho_s}{\frac{r}{r_s}\left(1+\frac{r}{r_s}\right)^n} \tag{3}$$

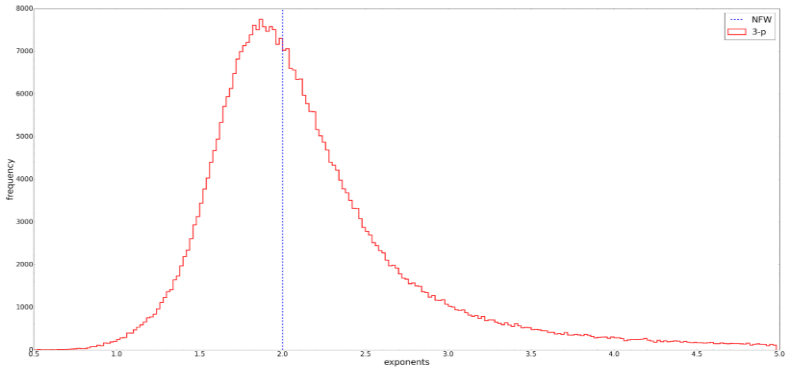

FIGURE 3. Distribution of Exponents from 3-Parameter Fit. The distribution of exponents, shown in red, peaks just before 2. The blue dotted line marks the NFW profile.

Optimizing the function for each of the more than 7 million halos at redshift $z = 0$ in the Bolshoi-Planck simulation is impractical without access to more processing power, so in the meantime, we ran the algorithm for the first 200,000 halos. Plotting a histogram of exponents from those halos, we found that the distribution still centers around 2, although it ranges from 0.5 to more than 4. While running the fitting algorithm, we also logged the "error" of each profile, which we defined as the sum of the squares of the residual at each radial bin:

$$error = \sum_{i=0}^{k} [\rho_i - \rho(r_i)]^2 \tag{4}$$

By graphing the relationship between exponent and error, we could see whether our new equation actually improved upon NFW. Although the errors were systematically larger at shallow outer slopes (smaller *n* values), they dropped quickly as *n* tended to 2, which represents NFW, and stayed largely the same as the slope grew steeper.

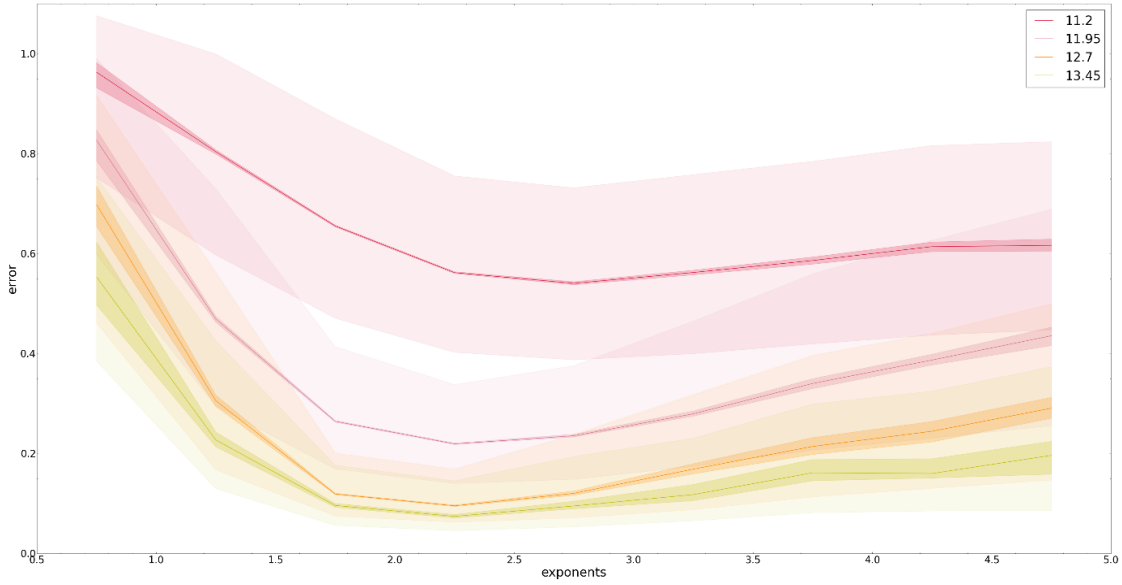

FIGURE 4. Error vs. Exponent. This plot shows that smaller exponents were generally correlated with worse fits. Larger exponents, however, had errors similar to the NFW error.

3.2 Checking Fits

In order to ensure that our analyses of the 3-parameter exponent would be accurate, we tested our fitting algorithm against the one used by Rockstar to calculate its NFW fit. The first result that we looked at was the distribution of all NFW r_s in the subset of halos that we optimized, and the distribution of NFW r_s from the halo catalog. If our optimization was indeed accurate, the general distribution of r_s values should look the same. As seen in Figure 4, however, the first test showed that the entire distribution of our values was shifted to the right of those from the catalog.

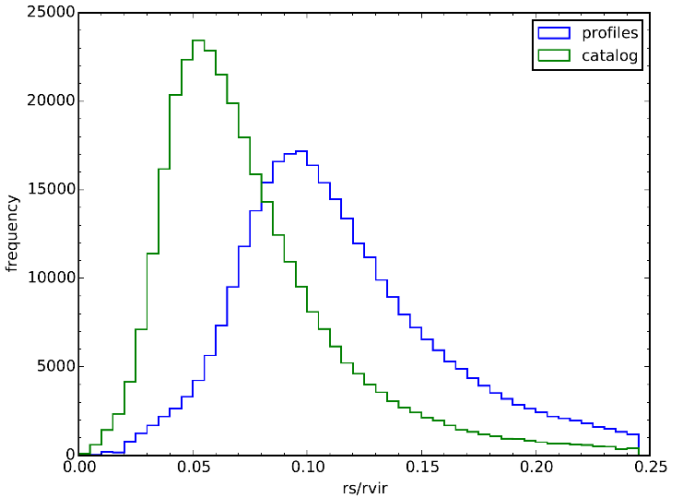

FIGURE 5. Distribution of NFW r_s. The normalized frequency of r_s values from our optimization algorithm, shown in blue, and the halo catalog, shown in green.

3.2.1 R_s by Optimization Inputs

In the creation of the Rockstar catalog, the first few radial bins are down-weighted for each halo to counteract the profiles' use of the log scale, which greatly emphasizes smaller radii. Without down-weighting, the fitting algorithm is likely to overestimate r_s because a larger portion of the graph lies within the scale radius. In order to replicate its effect, we tried running our fitting function again with the first bin and the first two bins removed from the input. Although both optimizations showed a closer resemblance to the catalog, they also showed a cluster of halos whose r_s values were suddenly very close to zero, which the catalog does not reflect.

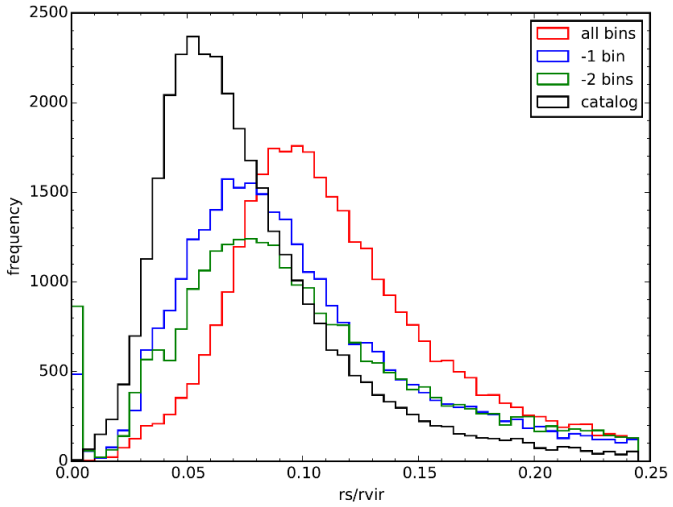

FIGURE 6. Distribution of NFW r_s from Different Optimizations. The normalized frequency of r_s values from the 3 optimizations, and the halo catalog (black). Although the -1 and -2 bin optimizations seemed more similar to the catalog, both exhibited a spike at the 0.0-0.005 bin.

3.2.1 R_s by Mass

Disregarding this discrepancy for the moment, we separated the halos by mass to see if the shift was prevalent at each mass bin. Because halos with lower masses have fewer particles in total, but the number of bins used is still similar to that of much more massive halos, each bin was likely to have fewer particles. This creates noise in the density distribution plots, which we hypothesized was a factor in the overestimation of r_s.

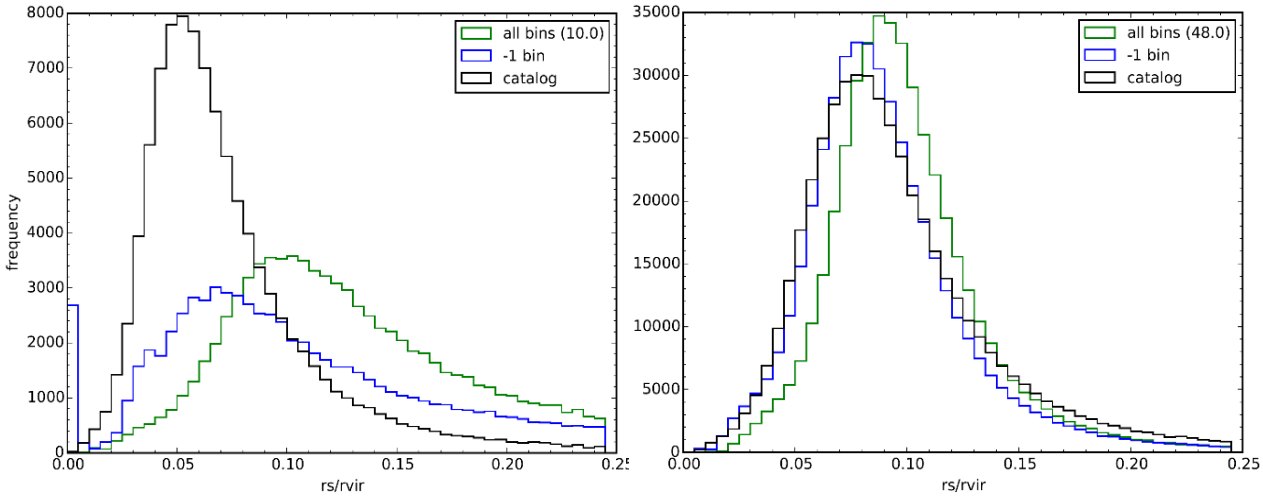

FIGURE 7. Distribution of NFW r_s by mass. The graph on the left shows the distribution for halos of mass 10^{10} - 10^{11} $M_\odot$, and the right shows the distribution for halos with mass >10^{11} $M_\odot$.

Indeed, only halos with $<10^{11}$ $M_\odot$ exhibited a pronounced rightward shift. Because there are many more halos at the lower mass ranges than at higher ones, this mass bin had an outsized effect on the overall distribution. Combined with the use of the -1 bin optimization, the distribution of our r_s values finally matched up with the catalog's. Coincidentally, removing the smallest halos also solved the issue of impossibly small r_s values. Because smaller halos have a smaller number of radial bins, the removal of the first bin leads the optimization algorithm to disregard much of the region within r_s.

3.2.3 3-Parameter Residual

In order to condense our large data set, we used the 3-parameter residual as another filter with which we could refine our analysis. Figure 8 shows that although most halos have a residual of less than 1.5, our optimization of the 3-parameter fit still did not show good agreement with a number of halos. Whether because of the algorithm itself, or the specific properties of the halo, those outliers would create noise in our results. Arbitrarily, we chose a cutoff at $1/5^{th}$ the peak of the distribution, which came out to be approximately 1.1, and excluded all halos with a residual greater than that. In only using halos with a mass greater than 10^{11} $M_\odot$ and residual less than 1.1, we reduced the number of halos in our analysis from 7 million to approximately 450,000.

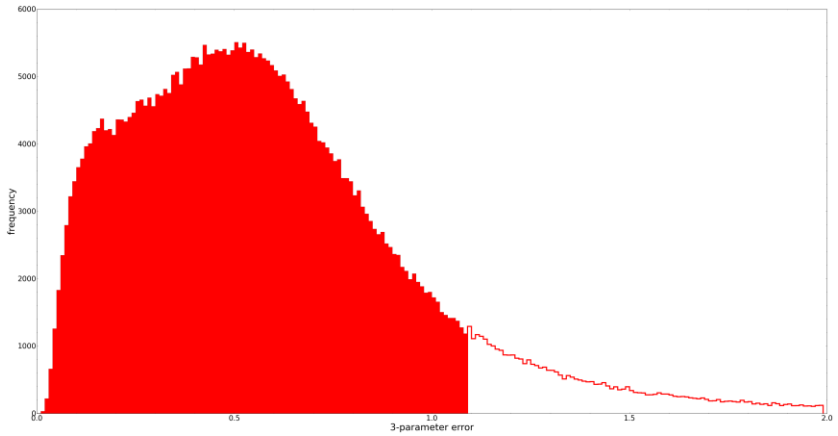

FIGURE 8. Distribution of 3-Parameter Residual. The frequency of residuals from the 3-parameter profile. We discarded all halos with error > 1.1.

3.3 Property Correlations

Finally, we could correlate the outer slope to the properties saved in the halo catalog. We ran the optimization algorithm again, this time filtering out the unfavorable halos beforehand, and matched up halo IDs from the halo profiles with their counterparts in the halo catalog. Then, we created a new catalog that comprised only the halos that we fitted. To the list of 92 halo properties that the catalog already held for each halo, we appended its NFW r_s, 3-parameter r_s, 3-parameter *n* value, and the residual from each profile.

In order to make comparisons between graphs easy, we largely standardized the graphing procedure for the correlations between outer slope and halo property. Although some properties were plotted on a log scale, and others on a simple linear scale, the exponent was always on the y-axis, and the halo property on the x-axis. Halos were separated into four mass bins, each of width $10^{0.75}$ $M_\odot$ in line with the results from Lee et al. (2016). X-values were binned differently for each property to minimize noise while not over-smoothing. In addition to the median n-value being plotted, the 25th and 75th percentile n-values were also shaded in. We also included a basic confidence interval, approximated from the binomial distribution, which is dependent on the number of halos in that bin (a):

$$percentile = a * 0.5 \pm 1.96\sqrt{a * 0.25} \mp 1 \quad (5)$$

4 RESULTS

Although we looked for a dependence on outer slope for a large number of properties, we found many that either showed no correlation, or were inconclusive. Although we have reason to believe that other properties are related to outer slope, only the properties discussed below had an explainable trend.

4.1 Concentration

The NFW concentration of a halo is defined as the ratio of a halo's virial radius to its scale radius, as calculated by the NFW profile. Although we were comparing values taken from different fits, the concentration is a good indicator of halo age. When halos first form, their concentrations are relatively low. As they grow, most of the mass is accreted into the outer regions of the halo, so the r_{vir} grows while r_s stays mostly constant. Thus, at a specified mass range, the higher the concentration of a halo, the more mass it has accreted, and the older it is relative to other halos of similar mass (Bullock et al. 2001). As Figure 10 shows, however, there is remarkable correlation between concentration and outer slope. We have yet to find an explanation for this phenomenon, but the evidence is indisputable.

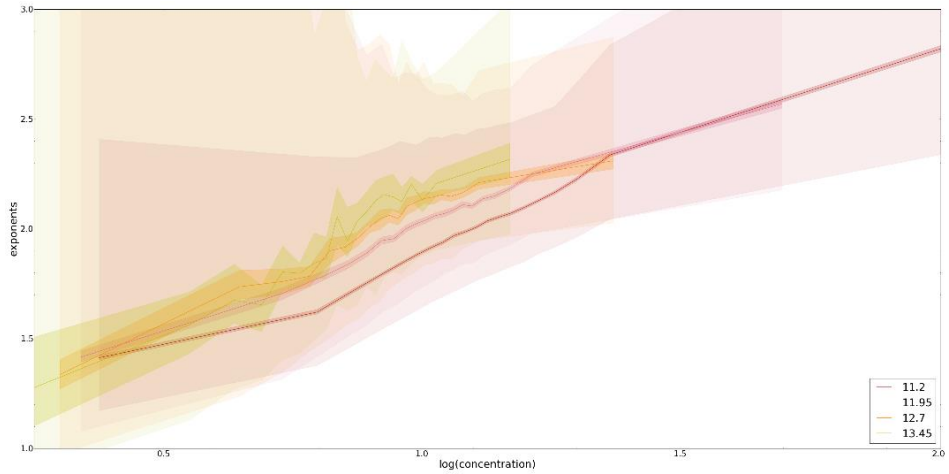

FIGURE 9. Exponent vs. Concentration. Exponent increases as concentration increases. Concentration is logged to focus on behavior at low concentrations.

4.3 Scale of Last Major Merger

The scale of last major merger is a scale factor measuring the time since a major merger between two halos, which is defined as a merger of two halos with a mass ratio greater than 0.3. The scale factor *a* represents the ratio of the distance between two halos at a previous timestep and

the distance now. Because the universe is constantly expanding, this ratio uses redshift to indicate the change in halo distance between the time of the merger and the present:

$$a = \frac{1}{1+z} \tag{6}$$

The larger the value, the more recently another halo has merged with the one in question. Because halos are constantly interacting with each other, smaller halos are often consumed by larger ones, which leads to the creation of larger and larger halos as the universe matures. We only looked at the most recent timestep, so all of the halos we analyzed had survived prior mergers.

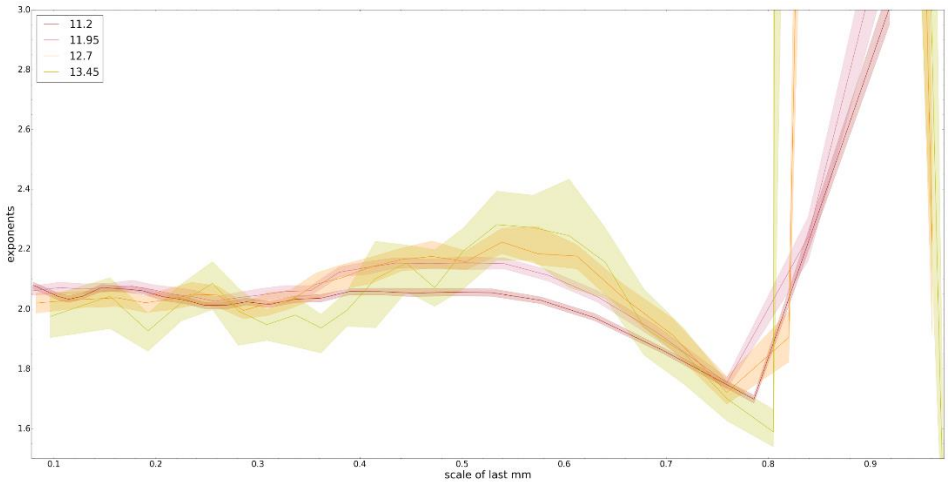

FIGURE 10. Exponent vs. Scale of Last Major Merger. Cusp at 0.8 scale factor where exponent is smallest. The 25th and 75th percentiles were not plotted because the range is too wide.

At all mass bins, we found a characteristic cusp at 0.8 scale factor that was followed by a gradual increase to the standard NFW exponent of 2. Halos that have recently undergone a merger, then, have the smallest slopes, before the accreted mass settles and the density distribution returns to normal. The exponent rises significantly as the scale factor nears 1, indicating a currently merging halo, and then drops suddenly. Although we have yet to explain that phenomenon, perhaps it can be attributed to the chaos that happens as halos collide and boundaries blur.

4.2 X-Off

The offset of a halo's density peak from its center of mass is its X-off. Because halos are stretched more along one axis as they evolve, it's quite often that the densest region of a halo is not exactly at its center. The larger the X-off, however, the more likely that mass is being accumulated in one region of the halo, creating a density peak farther away from the center. After plotting its correlation with outer slope, we found that high X-offs are correlated with small exponents. This is to be expected, because as mass is accreted, a region of high particle density should form away from the center of the halo. Because our bins are created as concentric spheres that radiate outward, the positions of particles within their shell are disregarded. This increase in mass at the outer region diminishes the density drop-off and generates a shallower slope. The position of the line also shifts to the right as mass increases: the higher the mass of the halo, the more likely it is to have a large X-off.

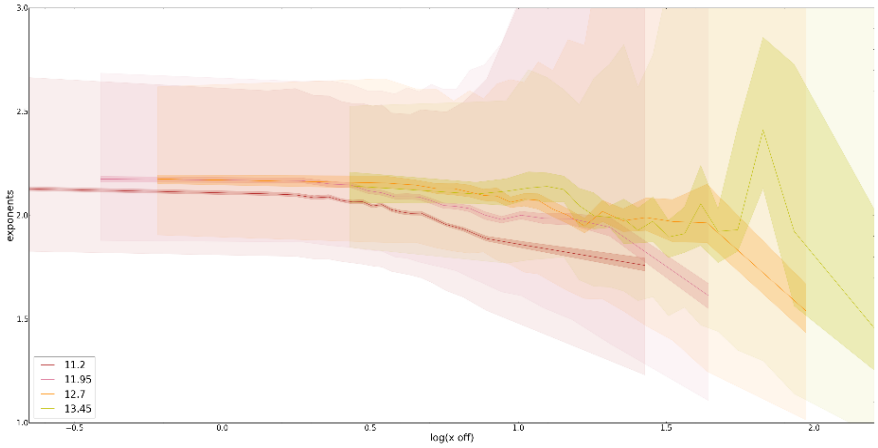

FIGURE 11. Exponent vs. X-Off. Exponent decreases as x-off increases. X-off is plotted on a log scale because most halos have low x-off.

4.4 Stripping

For the subset of halos that have lost mass during their lifetimes, the ratio of current mass to peak mass is the percent of stripping. As expected, halos in the smallest bin had the greatest stripping, because their low mass translates to a small Hill Radius. Halos that had been minimally

stripped had outer slopes similar to unstripped halos, but the more mass a halo had lost during its lifetime, the greater its exponent was. Because particles in the outer region of the halo are easier to strip, this relationship was expected. As the steady slope suggests, particles near the center of the halo are minimally affected even as more and more mass is stripped from the outer parts of the halo. Furthermore, the slopes of the lines increase as mass decreases, suggesting that this effect is more pronounced at lower masses.

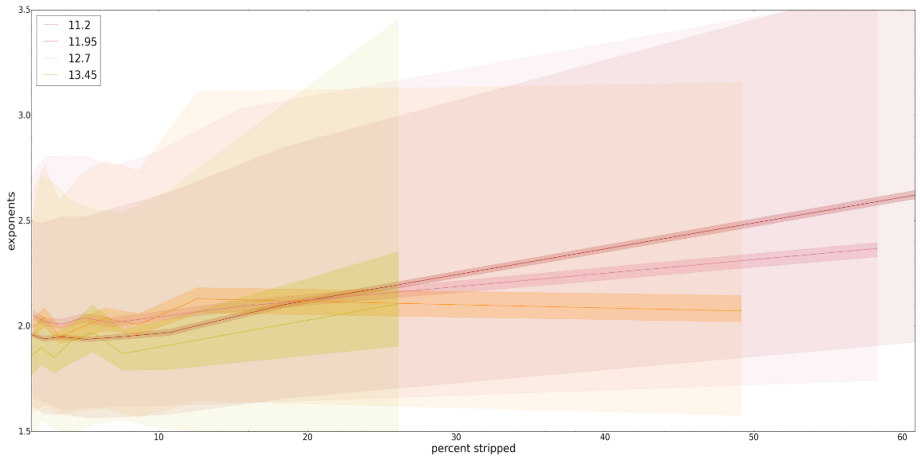

FIGURE 12. Exponent vs. Stripping. Exponent increases as stripping increases. The outer slopes of lower mass halos are more greatly affected by stripping, as the slope of the graph shows.

4.6 Local Cosmic Density

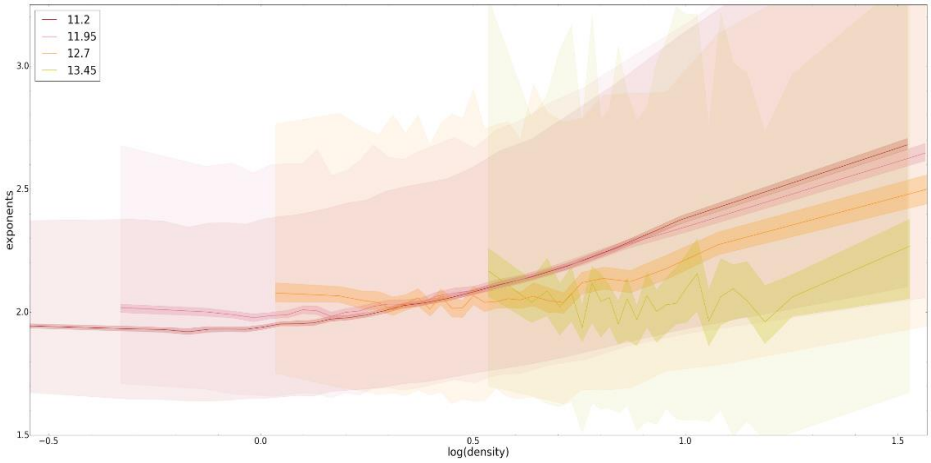

FIGURE 13. Exponent vs. Density. Exponent increases as local cosmic density increases. Like stripping, the effect is more pronounced at lower masses.

The local cosmic density is the density of dark matter particles in the region around a halo. The type of web feature that the halo is located in largely determines this: voids are regions of very low density and very few halos; walls, which appear where voids meet, have a moderate density; filaments, which are the intersections of two walls, higher density; and nodes, where multiple filaments cross, are the highest average density web structure. As Figure 13 shows, there is strong correlation between density and outer slope. While halos in low-density regions have exponent values, the exponent grows as density increases. Although the behaviors are similar, the greater the mass, the greater is the density threshold at which the exponent begins to increase.

We also looked at the quality of fit for halos with different densities. This time, instead of mass bins, we created five density bins, each 20 percentiles apart. Creating histograms of both the 3-parameter error and NFW error, we found correlations between density and fit error. Both profiles performed similarly well at the median density bins, and more poorly at the lowest mass bin. Worst, however, was the performance of NFW on halos in the highest density bin. Not only was the distribution shifted to the right, its peak was much lower than that of any other density bin, and the tail extended further to the right.

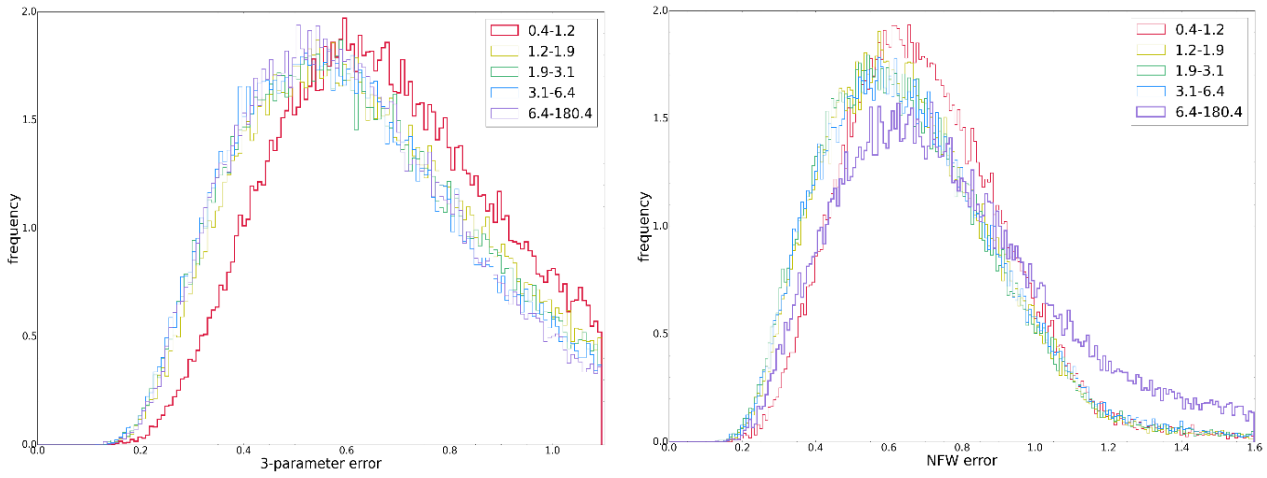

FIGURE 14. Distribution of 3-Parameter and NFW Residuals by Density. The graph on the left shows 3-parameter error, with the smallest density bin bolded. The distribution ends at 1.1 because of our cutoff value. The graph on the right is NFW error, with the highest density bin bolded.

5 DISCUSSION

Using a new profile that we derived from the classic NFW function, we present a way of characterizing the outer region of a dark matter halo that allows us to explore relationships between a halo's density distribution and its other properties. Given our robust procedure of filtering and sorting halos, we can conclude strong correlations between a halo's outer slope and its environment. Although further research is sure to discover correlations with other properties that are dependent on or describe halo's environment, our work has already produced results that provide descriptions of the types of halos that do not conform to the NFW profile. The one result that we have yet to explain is concentration. The relationship is strong enough that we included it in our results, but whether that emerges from the definition of NFW concentration, or its implications about halo age, is still a question to be answered.

5.1 Shallow Outer Slope

Our findings showed that halos with small exponent are typified by high x-offs and large scale factors of last major merger. From the latter of the two, we can deduce that recently merged halos have the shallowest slopes. Whether by collision or tidal halo destruction, it is the mass from the secondary halo that reduces the density drop-off in the primary halo, which is the one that we analyze. This is explained by the high X-off, which indicates a region of high density away from the primary halo's center of mass. In this case, the high density is a result of the stream of particles that the primary halo has created out of its satellite halo as they merge. The rightward shift of the X-off graph as halo mass increases also supports this point. Because larger-mass halos have larger tidal forces and are more likely to be the primary halo in a system, more of them have recently undergone a major merger that results in this behavior. As time passes, the new mass settle into place in the halo, X-off decreases, and the halo density distribution returns to normal.

5.2 Steep Outer Slope

For halos with steep outer slopes, we found that they exhibited high stripping and were located in highly dense regions. From Figure 13, we can infer that these halos had been tidally stripped. This phenomenon is more likely to occur in low-mass halos because of their low Hill Radii, and we see from the plot that while the maximum stripping experienced by halos in the highest mass bin was less than 30%, some halos in the lowest mass bins had been stripped upward of 60%. Similar behavior was found in Figure 14. For the highest-mass halos, the median exponent stays largely constant even as density increases, because they are likely the primary halo in a system. These large halos are found in high-density environments, because the short distances between halos translate to small Hill Radii, large tidal forces, and high mass accretion rates, either through stripping or mergers. Less massive halos, however, are susceptible to tidal stripping. As density increases, tidal forces from nearby halos more likely to create $R_{Hill} < R_{vir}$, and so low-mass halos in high-density regions have higher exponents, and are more stripped.

5.3 Quality of Fit

From our investigation of profile residuals at different densities, we discovered that each profile has its limitations. Both NFW and the 3-parameter profile fit halos at the lowest densities poorly. The similarity in these two profiles' error at this density bin—the 3-parameter error is slightly, but insignificantly, larger—can be explained by looking to Figure 15. At low densities, the exponent found by optimizing our 3-parameter profile is around 2, which makes the function equivalent to NFW. As density increases, though, only our profile can account for the steepening density drop-off caused by high stripping. For this reason, NFW performs much more poorly at the highest density bin than the 3-parameter profile, and more poorly than at any other density.

6 CONCLUSION AND FUTURE WORK

The recent advent of high-resolution cosmological simulations has given researchers fresh insight into the interactions that occur between dark matter halos. Harnessing the power of these supercomputers to simulate individual halos and their interactions at a large scale, we developed a way of characterizing the outer slope of a halo's density distribution, and examined the effects of halo environment on density distribution, through the lens of properties that are known to be dependent on environmental factors. Our 3-parameter fit is not meant to replace the NFW profile; in fact, our results reaffirm its general accuracy. What our function does allow us to do, however, is investigate those cases in which halos no longer agree with NFW. In our research, we have found two cases: halos that have been highly stripped, and halos that have recently undergone a merger. Because small halos are more susceptible to tidal stripping and destruction through mergers, in a high density environment, higher-mass halos are more likely to have an exponent less than 2, and lower-mass halos are more likely to have an exponent greater.

In the future, we hope to include halos with masses $<10^{11}$ $M_{\odot}$ in our analysis, and test whether our conclusions still stand. We will examine further the connection between slope and concentration and look for correlations with other halo properties. We are interested in whether additional sources of steeper and shallower slopes exist. Also, there are likely other cases in which the halo profile is affected by environment, and so we must also design new profiles targeted at finding halos that deviate from NFW in different ways, or perhaps even replace it. As computers continue to improve, and processing power continues to grow, new simulations are sure to help researchers gain a better understanding of interactions between dark matter halos.

.

References

[1] Behroozi, P., Wechsler, R., Wu, H. 2013, AJ, 1, 3, 5

[2] Klypin, A., Yepes, G., Gottlber, S., Prada, F., & He, S. 2014, MNRAS, 1

[3] Prada, F., Klypin, A., Cuesta, A., et al. 2012, MNRAS, 3018, 3021, 3025

[4] Blumenthal, G., Faber, S., Primack, J., & Rees, M. 1984, Nature, 517

[5] Schramm, D. 1993, AA, 13

[6] Allgood, B., Flores, R., Primack, J., et al. 2006, MNRAS, 1781, 1784, 1794

[7] Correa, C., Wyithe, J., Schaye, J., & Duffy, A. 2015, MNRAS, 1514

[8] Navarro, J., Frenk, C., & White, S. 1996, AJ, 564, 567, 574

[9] Navarro, J., Frenk, C., & White, S. 1997, ApJ, 462, 563

[10] Rodriguez-Puebla, A., Behroozi, P., Primack, J., et al. 2016, MNRAS, 462, 893

[11] Behroozi, P., Wechsler, R., & Wu, H.-Y. 2012, Astrophysics Source Code Library, 10008

[12] Taylor, J., Babul, A. 2001, ApJ, 559, 716

[13] Taylor, J., Babul, A. 2004, MNRAS, 348, 811

[14] Hahn O., Porciani, C., Dekel, A., et al. 2009, MNRAS, 398, 1742

[15] Hearin, A., Behroozi, P., van den Bosch, F. 2016, MNRAS

[16] Kampakoglou, M., Benson, A. 2007, MNRAS, 374, 775

[17] Benson, A. 2010, Physics Reports, 495, 33

[18] Lee, C., Primack, J., Behroozi, P. 2016, to be published

[19] Bullock J. S., Kolatt T. S., Sigad Y., et al. 2001, MNRAS, 321, 559